Alcohol reverses the effects of *KCNJ6* (GIRK2) noncoding variants on excitability of human glutamatergic neurons

Running title: Alcohol reverses effects of *KCNJ6* SNPs on neurons

Dina Popova[1], Isabel Gameiro-Ros[2], Mark M. Youssef[3], Petronio Zalamea[1], Ayeshia D. Morris[4], Iya Prytkova[2], Azadeh Jadali[3], Kelvin Y. Kwan[3], Chella Kamarajan[5], Jessica E. Salvatore[6], Xiaoling Xuei[7], David B. Chorlian[5], Bernice Porjesz[5], Samuel Kuperman[8], Danielle M. Dick[9], Alison Goate[10], Howard J. Edenberg[11], Jay A. Tischfield[1], Zhiping P. Pang[1,12], Paul A. Slesinger[2] and Ronald P. Hart[1,3,*]

Affiliations:

[1]Human Genetics Institute, Rutgers University, Piscataway, NJ 08854
[2]Nash Family Department of Neuroscience, Icahn School of Medicine at Mount Sinai, New York, NY 10029
[3]Department of Cell Biology & Neuroscience, Rutgers University, Piscataway, NJ 08854
[4]Joint Program in Toxicology, Rutgers University, Piscataway, NJ 08854
[5]Dept. of Psychiatry & Behavioral Sciences, SUNY Downstate Health Sciences University, Brooklyn, NY 11203
[6]Department of Psychiatry, Rutgers Robert Wood Johnson Medical School, Rutgers University, Piscataway, NJ 08854
[7]Department of Medical and Molecular Genetics, Indiana University School of Medicine, Indianapolis, IN 46202
[8]Department of Psychiatry, University of Iowa Carver College of Medicine, Iowa City, IA 52242
[9]Rutgers Addiction Research Center, Robert Wood Johnson Medical School, Rutgers University, Piscataway, NJ 08854
[10]Department of Genetics & Genomic Sciences, Icahn School of Medicine at Mount Sinai, New York, NY 10029
[11]Department of Biochemistry and Molecular Biology, Indiana Univ School of Medicine, Indianapolis, IN 46202
[12]Child Health Institute, Robert Wood Johnson Medical School, Rutgers University, New Brunswick, NJ 08854

*Corresponding author:
Rutgers University
Department of Cell Biology & Neuroscience
604 Allison Rd
Piscataway, NJ 08854

(848) 445-1783
rhart@rutgers.edu

Abstract

Synonymous and noncoding single nucleotide polymorphisms (SNPs) in the *KCNJ6* gene, encoding G protein-gated inwardly rectifying potassium (GIRK2) channel subunit 2, have been linked with increased electroencephalographic frontal theta event-related oscillations (ERO) in subjects diagnosed with alcohol use disorder (AUD). To identify molecular and cellular mechanisms while retaining the appropriate genetic background, we generated induced excitatory glutamatergic neurons (iN) from iPSCs derived from four AUD-diagnosed subjects with *KCNJ6* variants ('Affected: AF') and four control subjects without variants ('Unaffected: UN'). Neurons were analyzed for changes in gene expression, morphology, excitability and physiological properties. Single cell RNA sequencing suggests that *KCNJ6* AF variant neurons have altered patterns of synaptic transmission and cell projection morphogenesis. Results confirm that AF neurons express lower levels of GIRK2, have greater neurite area, and elevated excitability. Interestingly, exposure to intoxicating concentrations of ethanol induces GIRK2 expression and reverses functional effects in AF neurons. Ectopic overexpression of GIRK2 alone mimics the effect of ethanol to normalize induced excitability. We conclude that *KCNJ6* variants decrease GIRK2 expression and increase excitability and that this effect can be minimized or reduced with ethanol.

63 # Introduction

64 Alcohol use disorder (AUD) is a heritable (h^2 = 0.49) condition characterized by an impaired
65 ability to stop or control alcohol use despite adverse social, occupational, or health
66 consequences[1]. An estimated 14.1 million American adults (ages 18+) were diagnosed with AUD
67 in 2019 and the numbers continue to grow, particularly due to the COVID-19 pandemic[2]. Even
68 though several evidence-based treatments are available for AUD[3-5], there is a high discrepancy
69 in treatment outcomes, suggesting the existence of a variety of traits influencing the
70 development of specific physiological and behavioral responses to alcohol. Understanding
71 biological factors, specifically genetic risk, at the level of neuronal function is fundamental to
72 developing tailored preventive interventions and better matching of patients to treatment.

73 The Collaborative Study on the Genetics of Alcoholism (COGA) collected a diverse set of
74 phenotypes, including electroencephalogram (EEG) parameters, in the search for genes and
75 endophenotypes associated with AUD[6,7]. A family-based, genome-wide association study
76 (GWAS) of a frontal theta event related oscillation (ERO) phenotype identified an association
77 with several single nucleotide polymorphisms (SNPs), including a synonymous SNP, rs702859, in
78 the *KCNJ6* gene on chromosome 21[8]. More recent studies concluded that this polymorphism
79 influences the magnitude and topography of ERO theta power during reward processing in a
80 monetary gambling task, reflecting a genetic link to neuronal circuits[9,10]. Two other SNPs
81 (rs702860 and rs2835872) within *KCNJ6* were linked with the ERO endophenotype and AUD,
82 but are noncoding, either intronic or within the 3' untranslated region (3' UTR), respectively.
83 Additional studies identified various genetic loci correlating with selected EEG results but all
84 consistently include alcohol dependence[11,12]. To understand how these SNPs might influence
85 these phenotypes, it is essential to characterize the pathways and mechanisms by which
86 genetic risk unfolds at molecular, cellular and network resolutions. Furthermore, since the
87 *KCNJ6* SNPs are non-coding or synonymous, the optimal strategy would incorporate human
88 genetic backgrounds of actual subjects to preserve potential effects of noncoding sequences.

89 *KCNJ6* encodes the G protein-gated inwardly rectifying potassium channel subunit 2 (GIRK2),
90 which, when assembled into a GIRK channel, plays a role in regulating cell excitability[13]. The
91 inward rectifying properties of GIRK are based on the ability to conduct potassium ions into the
92 cell more easily than out, leading to a reduction in excitability[14,15]. GIRK function in neurons is
93 associated with activation of G protein-coupled receptors (GPCRs), which leads to dissociation
94 of Gβγ subunits from the G protein complex and binding to the channel[16]. In addition, this
95 family of GIRK channels can be potentiated by ethanol concentrations (20-50 mM) relevant to
96 human alcohol usage through direct interaction with a hydrophobic pocket on the channel[17,18].
97 Studies in model organisms also reveal the importance of GIRK function in AUD: mice lacking
98 GIRK2 demonstrate reduced ethanol analgesia, greater ethanol-stimulated activity in open-field
99 tests, increased self-administration of ethanol, and failure to develop a conditioned place
100 preference for ethanol[19-21]. Thus, GIRK channels not only modulate the excitability of the
101 neurons but also play an essential role in regulating responses to alcohol.

102 Recent studies have employed the use of subject-specific induced stem cell technology to
103 model, characterize and elucidate mechanisms underlying various types of addiction disorders
104 including AUD[22-25]. The generation of specific subtypes of cultured human neurons enables the
105 study of formerly inaccessible functional properties using standard neuroscience methods[22,24-
106 26]. The contribution of various *KCNJ6* SNPs was found to affect a variety of properties
107 associated with neuronal function or sensitivity to drugs of abuse, suggesting targets for
108 potential therapeutic interventions. Associating specific genetic variants with mechanisms
109 contributing to addictive behaviors may produce more effective therapies tailored to individual
110 genotypes.

111 We hypothesize that noncoding SNP variants in *KCNJ6* alter neuronal excitability, potentially
112 contributing directly or indirectly to network-level endophenotypes such as ERO. Furthermore,
113 since ethanol interacts directly with GIRK2, we predict that excitability will be modulated by
114 ethanol. To test these hypotheses, we evaluated a human neuron model system that includes
115 variant genotypes, so that specific intergenic or noncoding sequences as well as genetic
116 backgrounds influencing these functions would be preserved. Therefore, we selected subjects
117 from the NIAAA/COGA Sharing Repository, four with the ERO-associated allelic variant in *KCNJ6*
118 and the presence of diagnosed alcohol dependence and four without the variant and
119 unaffected for AUD and produced eight iPSC lines. iPSCs were reprogrammed into excitatory
120 human neurons (iN) to investigate the potential contribution of the *KCNJ6* SNPs to AUD
121 diagnosis and the ERO power endophenotype (Fig. 1A). We found that neurons from *KCNJ6*
122 variant AUD-affected individuals demonstrated initial transcriptomic and morpho-physiological
123 differences, mostly affecting excitability of the cells, which were paralleled by differences in
124 GIRK2 expression levels. Ethanol exposure, conversely, induced GIRK2 expression, ameliorating
125 differences in excitability. Moreover, by overexpressing *KCNJ6* we replicated effects of ethanol
126 on neuronal excitability. The results promote a better understanding of the association
127 between genetic variants and brain-wide changes affecting AUD risk and can potentially be
128 used for development of personalized interventions.

129

130 # Methods

131 **Generation of human iPS cells and glutamatergic neurons (iN)**
132 Subjects were selected from the NIAAA/COGA Sharing Repository of the Collaborative Study on
133 the Genetics of Alcoholism (COGA) project with characteristics summarized in Table 1. Selection
134 criteria consisted of *KCNJ6* SNP genotype, DSM IV diagnosis of AUD, sex, and availability of
135 frozen lymphocytes in the repository. All subjects were of European ancestry. See
136 **Supplemental Methods** for details. The previously-described protocol for generating
137 glutamatergic human induced neurons (iN)[27-29] was modified. To obtain cultures with enhanced
138 levels of spontaneous activity, we minimized the time of Ngn2 induction to reduce alternate
139 cell identities[30] and fed cultures with a low-molality medium for at least 30 days post-
140 induction[31] as described in the **Supplemental Methods**. Cultures of iN typically exhibited resting
141 membrane potentials averaging -40 mV with the presence of synaptic markers, spontaneous
142 action potentials, and synaptic activity.

143 **Intermittent Ethanol Exposure (IEE).**
144 Since ethanol evaporates during culture incubation (Supplemental Figure 7), we added ethanol
145 to 20 mM and then replenished half the medium daily with 40 mM ethanol. Ethanol
146 concentrations were measured using an AM1 Alcohol Analyzer (Analox Instruments, Ltd.)[25].

147 **RNA sequencing**
148 For bulk RNAseq, individual iN cultures were harvested in lysis buffer and column purified
149 (Quick-RNA kit, Zymo). RNA was sent to Novogene, Inc., for sequencing. Analysis is described in
150 the **Supplemental Methods**. RNAseq data have been deposited with the NIH GEO repository
151 (accession number GSE196491). For single-cell RNA sequencing (scRNAseq), iN cultures were
152 treated for 7 days using IEE[25] starting 21 days after plating onto glia. At 28 days, iN were
153 dissociated using trypLE Express (Thermo Fisher) for 5 minutes at 37°C and then processed and
154 analyzed as described in the **Supplemental Methods**. These data have been deposited with the
155 NIH GEO archive, accession number GSE203530.

156 **Electrophysiology**
157 Analyses of iN used whole-cell patch-clamp electrophysiology as previously described[24,25] with
158 details provided in the **Supplemental Methods**. Drugs were applied through a perfusion system
159 in the following concentrations: 160 nM ML297 or 20 mM ethanol. Clampfit software (pClamp
160 11; Molecular Devices) was used for analysis of recordings.

161 **Immunocytochemistry and confocal imaging**
162 iN cultures were fixed for 30 min in ice cold methanol and permeabilized using 0.2% Triton X-
163 100 in PBS for 15 min at room temperature. Cells were then incubated in blocking buffer (5%
164 BSA with 5% normal goat serum in PBS) for 30 min at room temperature and then incubated
165 with primary antibodies diluted in blocking buffer overnight at 4°C, washed with PBS three
166 times, and incubated with secondary antibodies for 1 h at room temperature. Confocal imaging
167 was performed using a Zeiss LSM700. Primary antibodies used: rabbit anti-GIRK2 (Alomone

168 labs, APC-006, 1:400), mouse anti-βIII-tub (BioLegend, MMS-435P,1:1000), chicken anti-MAP2
169 (Millipore AB5543, 1:1000), mouse anti-Syn1 (SYSY,106-011, 1:200), mouse anti-PSD 95 (SYSY,
170 124-011, 1:2000), mouse anti-mCherry (Thermofisher Scientific, M11217, 1:100).

171 **Fluorescent in situ hybridization (FISH)**
172 Fluorescent, single molecule *in situ* hybridization was performed with the RNAscope® Multiplex
173 Fluorescent Detection Kit v2 (Advanced Cell Diagnostics, ACD) following the manufacturer's
174 instructions and details provided in the **Supplemental Methods**.

175 **Image analysis**
176 Cytometric analysis was performed using the Fiji/ImageJ image analysis program[32] as described
177 in the **Supplemental Methods**. ImageJ scripts can be downloaded from
178 https://github.com/rhart604/imagej. The person performing analysis was blinded to genotype
179 or line information.

180 **Lentiviruses**
181 FSW-hSyn-GCaMP6f assembly was described previously[33]. FUGW-KCNJ6-mCherry was
182 assembled using lentiviral backbone from FUGW (AddGene #14883), *KCNJ6* coding sequence
183 amplified from human neuron cDNA (forward primer: agccaggaaaagcacaaaga, reverse primer:
184 ggggagaagagaagggtttg), and mCherry with a nuclear localization signal from pME-nlsmCherry (a
185 gift from Dr. Kelvin Kwan). During construction, the GIRK2 protein-coding sequence was tagged
186 with a 3xHA tag and linked to mCherry with a T2A "self-cleaving" element.

187 **Calcium imaging in iPSC-derived iN populations**
188 For assessing neuronal excitability, iN co-cultured with mouse glia on Matrigel™ coated 10 mm
189 glass coverslips were transduced with lentivirus expressing hSyn-GCaMP6f at least 2 weeks
190 prior to imaging to ensure robust expression. All fluorescence imaging experiments were
191 performed in ~50 DIV (days in vitro) iNs. Details of the protocol and analysis are found in the
192 **Supplemental Methods**.

193 **Statistics**
194 Parameters that were sampled in cells from multiple microscopic fields and from multiple cell
195 lines were fit to a linear mixed-effects model using the lme4 package in R[34]. The model included
196 the cell line identifier and sex. A Tukey post-hoc test identified pairwise differences in two-
197 factor models (e.g., genotype and ethanol). Electrophysiology results were modeled using
198 generalized estimating equations (GEE) with the cell line as grouping identifier using the
199 geepack R package[35]. Where appropriate, ANOVA or Student's t-test was used as indicated in
200 figure legends. For RNAseq, pseudo-bulk data (single cell reads pooled by subject identifier)
201 were modeled in DESeq2[36], testing first by likelihood ratio testing (LRT) over all groups, and
202 then pairwise comparisons were evaluated using Wald tests. After Benjamini-Hochberg
203 multiple measurements correction, a false discovery rate of 5% was set as a threshold for
204 significance. Numbers of replicate cells and/or fields per cell line and genotype used for
205 statistical testing are listed in Supplemental Table 6.

206 # Results

207 **Gene expression predicts functional differences between *KCNJ6* haplotypes**
208 To investigate the role of *KCNJ6* gene variants in neuronal function and ethanol response we
209 selected eight subjects of European ancestry from the COGA cell repository, with contrasting
210 *KCNJ6* SNPs and the presence or absence of alcohol dependence (Table 1). Since multiple SNP
211 genotypes were used, we label groups as AUD "affected" (**AF**) or "unaffected" (**UF**) for
212 simplicity, since in this set of subjects diagnosis correlates with SNP haplotype. However, the
213 focus of this study is the *KCNJ6* haplotype.

214 To confirm and extend SNP genotypes, iN cultures were harvested for bulk RNAseq analysis. To
215 identify isoforms, RNAseq data identified only the longer *KCNJ6* isoform ENST00000609713 (Fig.
216 1B), which includes a 3' exon of 18,112 nucleotides primarily consisting of 3'UTR. We identified
217 19 additional 3'UTR SNPs linked with the initial three (Supplementary Table 1; red lines in Fig.
218 1B), constituting a haplotype of 22 variants (synonymous and noncoding) within the expressed
219 isoform of *KCNJ6* mRNA, all in a region of linkage disequilibrium (LD; Supplemental Figure 1C).
220 There are no nonsynonymous variants, therefore, this haplotype is predicted to alter *KCNJ6*
221 mRNA stability, translation, or other post-transcriptional processes.

222 Previous studies suggested that iN cultures may be heterogeneous, potentially confounding a
223 bulk RNAseq analysis[30]. To enable analysis of iNs, we used single-cell RNAseq (scRNAseq) of
224 pooled neurons from multiple cell lines, a strategy known as a "cell village[37]." Based on
225 preliminary results indicating differences in excitability, we cultured each haplotype separately
226 to avoid potential secondary effects, combining cells each group in equivalent proportions.
227 Following maturation (~30 days after induction), dissociated cells were processed to generate
228 scRNAseq libraries. Mapping cells by t-distributed stochastic neighbor embedding (tSNE), a
229 distinct cluster of cells coordinately expressed several markers consistent with neuron
230 physiological function (Fig. 1C and Supplemental Fig. 2E), including synaptophysin (*SYP*),
231 voltage-gated sodium channel (*SCN3A*), glutamate transporter (*SLC17A6*), and both NMDA
232 (*GRIN2A*, *GRIN2B, GRIA2, GRIA4*) and kainate glutamate receptors (*GRIK2*). This cluster also
233 expressed both *KCNJ6*, encoding GIRK2, and *KCNJ3*, encoding GIRK1, which are required to form
234 heterotetrameric, functional channels[14,38]. Detection of mRNA in individual cells by scRNAseq
235 underestimates expression, so the cluster identified as neurons likely expresses markers more
236 uniformly than observed here. We conclude that this cluster of cells expresses components
237 required for physiological activity, and that other cells, expressing subsets of these neuronal
238 markers, are alternate products of induction, which we label as "transitional" neurons (Fig. 1C),
239 since reprogramming is not identical to differentiation[39,40]. Therefore, we focused gene
240 expression analysis on the phenotypically neuronal subset of cells.

241 Cells from individual subjects were distinguished by expressed SNPs[41], and sequencing reads
242 from each subject were combined to create a "pseudo-bulk" analysis, treating each subject and
243 treatment condition as replicates. Comparing the untreated AF group with the untreated UN

244 group, we identified 797 up-regulated genes, and 596 down-regulated genes (Fig. 1D;
245 Supplemental Table 3). Examining the results for differences by sex instead of *KCNJ6* haplotype
246 identified only 6 genes, 4 of which are encoded on X or Y, indicating that the sex of the samples
247 did not substantially contribute to gene expression differences. Gene ontology analysis of the
248 down-regulated genes (Fig. 1E; Supplemental Table 4-5) predicts several biological processes
249 associated with nervous system development, axonal transport, and trans-synaptic signaling. By
250 grouping enriched gene ontology terms by their parent terms (Supplemental Fig. 3), the major
251 themes in the down-regulated genes (Supplemental Table 5) are synaptic signaling and neuro
252 projection morphogenesis. Up-regulated genes (Supplemental Table 4) predict functions
253 associated with protein targeting within the cells, catabolic metabolism, and nonsense-
254 mediated decay. *KCNJ6* mRNA trended lower in untreated AF than in UN (Fig. 1C; $p = 3.15 \times 10^{-5}$
255 by LRT over both genotype and ethanol treatment; $p = 0.0508$ for untreated AF vs. UN by Wald
256 test). Interestingly, 7 d of IEE increased levels of *KCNJ6* mRNA (Fig. 1C; $p = 0.0225$, Wald test) so
257 that the treated AF group was no longer different from untreated UN ($p = 0.322$; Wald test).
258 Analysis by sex identified no significant differences in *KCNJ6* mRNA. Results indicate that the
259 variant *KCNJ6* haplotype leads to differential expression of GIRK2 and that ethanol exposure
260 will reverse these effects.

261 **GIRK2 expression and function in iPSC-derived induced excitatory human neurons (iN)**
262 Given the differences in gene expression and partial reversal of KCNJ6 downregulation, we
263 evaluated detailed neuronal phenotypes in UN and AF iN cultures, including GIRK2 expression,
264 neuronal morphology, and physiological response. Since GIRK2 immunocytochemistry had not
265 been reported in cultured human neurons, we validated detection using mouse primary cortical
266 cultures[42] (Fig. 2A-B). Lentiviral-transduced GIRK2 overexpression increased levels of
267 immunostaining about 3.5-fold (Fig. 2C, $mCherry^{+}$ cells are KCNJ6 lentiviral-transduced).
268 Importantly, silencing KCNJ6 with shRNAs or frameshift knockout by CRISPR/Cas9 eliminated
269 GIRK2 immunoreactivity (Supplemental Fig. 4B,C), which further confirms antibody specificity.

270 To confirm that GIRK2 expression contributes to potassium channel function, we treated iN
271 cultures with ML297, a selective activator of the GIRK1/GIRK2 heterotetramer complex[43,44].
272 Results show that the magnitude and frequency of native (basal) currents observed in human iN
273 were relatively small (Fig. 2D.b), with only 6.8% of the neurons responding to a shift in
274 membrane potential holding current (~10 pA). However, cells overexpressing GIRK2 (identified
275 by mCherry co-expression; Fig. 2D.c), exhibited an increased frequency of response (GIRK
276 currents) to 30% of the cells after ML297 addition (Fig. 2D.b) without a change in magnitude
277 (Fig. 2D.e). Importantly, GIRK activation affected excitability of the neurons by shifting resting
278 membrane potential to more negative values (Fig. 2D.d), affecting the ability of neurons to fire
279 APs when induced (Fig. 2D.f). We conclude that increased *KCNJ6* expression affects neuronal
280 excitability by altering GIRK channel activity.

281 ***KCNJ6* haplotype alters morphology and membrane excitability**
282 To identify neuronal properties affected by *KCNJ6* haplotype, we focused on three aspects:
283 morphology, expression of GIRK2, and basal physiological properties. A detailed analysis of
284 neuronal morphology is essential to rule out differences affecting excitability[45]. Most measures
285 of basic neuronal morphology did not exhibit differences by haplotype, including soma size,
286 circularity, and solidity, which describe the most fundamental aspects of neuron shape (Fig.
287 3B.a-c). However, neurite area, as determined by βIII-tubulin-staining, reflecting the number
288 and/or branching of neurites per cell, increased in the AF group (p =0.018; Fig. 3B.d), with
289 example images from individual cell lines in Figure 3C. Results are plotted for each cell line or
290 aggregated by *KCNJ6* haplotype. As predicted by *KCNJ6* mRNA expression (Fig. 1J), GIRK2
291 immunoreactivity was decreased in the AF group (Fig. 3D), measured by puncta counts (p =
292 0.0012; Fig. 3D.a), puncta circularity (p =0.007; Fig. 3D.c), and solidity (p = 0.037; Fig. 3D.d) but
293 not puncta size (Fig. 3D.b). No difference was found by sex. These results demonstrate an
294 overall decrease in GIRK2 in neuronal processes in the AF (*KCNJ6* variant allele) group.

295 Reduced GIRK2 expression is predicted to affect the excitability of neurons. As expected, we
296 found no differences in membrane capacitance, membrane resistance, spontaneous excitatory
297 post-synaptic potential (sEPSC) frequencies or amplitudes, or spontaneous action potential (AP)
298 firing (Fig. 3F). However, we observed increased excitability in the AF group ($p = 1.2 \times 10^{-5}$, Fig.
299 3G). Less current injection, using a ramp technique, was required for the AF group to shift the
300 resting membrane potential (RMP) of neurons held at -65 mV, producing more AP firing,
301 compared with the UN group ($p = 2.0 \times 10^{-9}$, Fig. 3G.d). Therefore, the *KCNJ6* variant haplotype
302 group (AF) exhibited increased neurite area, reduced neurite GIRK2 expression, and greater
303 excitability. Other neuronal properties were unchanged, suggesting that overall neuron
304 differentiation status was similar.

305 Since cultures are heterogeneous (Fig. 1C), we wished to evaluate larger sample sizes.
306 Therefore, we used calcium imaging to assess spontaneous and glutamate-stimulated firing. We
307 selected four cell lines for these studies (AF: 233 and 246, and UN: 420 and 472) and used the
308 viral-transduced, genetically-encoded calcium indicator GCaMP6f as a proxy for neuronal
309 activity[46]. Example images show consistent expression in all cell lines (Fig. 4A). Cultures were
310 treated with repeated pulses of 10 μM glutamate (each followed by wash-out with ACSF), and
311 one pulse of 50 μM glutamate to elicit transient increases in fluorescence, indicating receptor-
312 induced excitability, followed by pulses of 18 mM KCl, indicating cellular excitability (Fig. 4B-D).
313 Neurons from both UN and AF groups had heterogeneous spiking patterns, with >50% of the
314 neurons remaining inactive during the baseline period or after stimulation with glutamate or
315 KCl. This is consistent with scRNAseq results indicating that only ~23% of the iN cells express
316 genetic markers consistent with excitability (Fig. 1C). Increased spontaneous and induced
317 spiking (> 1-2 spikes) was apparent in the AF group when viewing individual cell responses in a
318 raster plot (Fig. 4B-C). Spiking frequencies increased 2.4-fold in baseline conditions (Fig. 4E; p =
319 1.1×10^{-6}) and 1.3-fold following glutamate stimulation (Fig. 4F; $p = 1.6 \times 10^{-3}$) in the AF group,

320 but no difference was found in KCl-induced activity (Fig. 4G; p = 0.85), confirming the above
321 results from individual neurons. When examining the AF or UN neurons individually, we also
322 observed higher spontaneous and glutamate-elicited excitability for lines 233 and 246 when
323 compared to line 472, which was found to be the least active spontaneously or under
324 glutamate stimulation among the four studied (Supp. Fig. 6). Overall, cells from the AF *KCNJ6*
325 variant allele group were more excitable, with no difference in basal physiological properties
326 (i.e., KCl-induced activity). Furthermore, not only did the spike rate increase per cell (bar plots,
327 Spikes/ROI/min), but we also observed increases in the proportion of cells in a field that
328 responded (pie plots). These results not only confirm findings of differences in excitability, but
329 also demonstrate that the difference in the AF iNs is found in not only individual cell activity but
330 also in the frequency of detecting active cells within a population.

331 **Ethanol exposure eliminates differences in properties affected by *KCNJ6* haplotype**

332 Analysis of *KCNJ6* mRNA expression in selected neurons (Fig. 1C) not only detected decreased
333 basal levels in the AF group, but also demonstrated increased expression following ethanol
334 treatment. This predicts that increasing GIRK2 expression in the AF group following ethanol
335 treatment would eliminate differences from the UN group in morphology, expression, and
336 physiology.

337 To control ethanol dosage in culture, we utilized an intermittent ethanol exposure (IEE)
338 paradigm as in previous studies[25]. Ethanol was replenished daily to account for loss by
339 evaporation, producing mean concentrations of 15.4 ± 1.16 mM (Supplemental Fig. 7). The half-
340 life of ethanol is 14.5 h (with a 95% CI of 13.5 to 15.6 h), so over 24 h the concentration would
341 drop to ~5-8 mM before replenishment. We targeted a peak concentration of 20 mM ethanol,
342 which is similar to a blood alcohol concentration (BAC) of 0.08% (17 mM), the legal limit for
343 intoxication. We also selected this concentration based on concentration-dependent
344 interactions of GIRK2 with ethanol[17]. After 7 days of IEE, we evaluated neuronal morphological
345 and functional properties. Focusing on parameters that were different by genotype without IEE
346 (Fig. 3&4), we found that ethanol eliminated the differences in total neurite area (p = 0.98, Fig.
347 5A.d), GIRK2 puncta counts (p = 0.46, Fig. 5B.a), excitation following current injection (p = 0.32,
348 Fig. 5E.a), step- (p = 0.48, Fig. 5E.b), and ramp- (p = 0.95, Fig. 5E.d) induced APs. Membrane
349 capacitance was slightly but significantly reduced in the IEE AF group ($p = 9.6 \times 10^{-9}$, Fig. 5D.a).
350 Other measurements were unchanged, again indicating that the cultured neurons exhibited
351 similar differentiation properties. Results are consistent with the interpretation that neurite
352 and excitability differences correlate with reduced GIRK2 expression, and that ethanol increases
353 expression of GIRK2, reversing these effects.

354 To confirm that both *KCNJ6* haplotype and ethanol exposure affect GIRK2 expression, we
355 evaluated GIRK2 immunocytochemistry and *KCNJ6* mRNA in neurons using fluorescent in situ
356 hybridization (FISH). GIRK2 increased following IEE ($p=1.0 \times 10^{-20}$, Fig. 5G-H). By probing *KCNJ6*
357 fluorescent puncta colocalized with MAP2 immunocytochemistry, we confirmed that neurons
358 from AF individuals had lower levels of *KCNJ6* mRNA compared to UN neurons (Fig. 5J.a, p = 8.2

359 x 10^{-3}). We also found that the proportion of $MAP2^{+}$ neurons expressing *KCNJ6* was reduced in
360 AF compared with UN (50.1% vs 64.7%, Fig. 5J.b), and the AF neurons had a greater proportion
361 of cells with low levels of expression (Fig. 5J.c) with no detectable High or Very High (>9
362 puncta/cell) expression. Differences in expression were found by haplotype in somatic regions
363 of neurons (Fig. 5J.f, $p = 5.5 \times 10^{-3}$) but not in non-somatic processes (Fig. 5J.g, $p = 0.23$). Ethanol
364 increased *KCNJ6* mRNA levels in both groups (Fig. 5J.a-e), eliminating the difference between
365 genotypes. Interestingly, we also observed that the proportions of AF neurons expressing
366 *KCNJ6* was increased (8.3%, Fig. 5J.b) by ethanol and was paralleled by a reduction in number of
367 low-expressing cells and increased appearance of high-expressing neurons (Fig. 5J.c). Results
368 indicate that variant *KCNJ6* haplotype leads to reduced *KCNJ6* expression, which is consistent
369 with RNA sequencing and immunocytochemical results, and that ethanol increases *KCNJ6*
370 expression, eliminating differences between haplotype groups.

371 **GIRK2 overexpression mimics IEE in human neurons with *KCNJ6* variants**

372 To test if ethanol-induced GIRK2 expression could underlie the elimination of differences in
373 neuronal properties associated with the *KCNJ6* haplotype, we compared ethanol treatment
374 with virus transduced *KCNJ6* overexpression. Since ethanol has been shown to potentiate
375 GIRK2-containing channels, we used a single treatment with 20 mM ethanol followed by
376 fixation 24 h later. As expected, neither ethanol nor GIRK2 overexpression exhibited differences
377 in passive neuronal properties. However, while current-induced activity increased in control
378 cultures ($p = 6.8 \times 10^{-6}$, Fig. 6C), no significant difference was found in cultures exposed to 24 h
379 ethanol ($p = 0.74$) and GIRK2 overexpression ($p = 0.23$). Similarly, while control cultures had
380 increased ramp-induced APs ($p = 5.9 \times 10^{-4}$; Fig. 6A) neither GIRK overexpression ($p = 0.14$) or
381 ethanol ($p = 0.10$) were significantly different. As a control, GIRK2 puncta count increased in a
382 sample cell line after overexpression (line 376, $p = 0.04$, Fig. 6D) without an increase in
383 circularity or solidity (not shown). These results indicate that the increased excitability in *KCNJ6*
384 minor allele haplotype cells is due to reduced expression of GIRK2 protein and this effect is at
385 least partially ameliorated or reversed by exposure to doses of ethanol found in human brain
386 after moderate to heavy daily drinking.

387

Discussion

This study focused on the effect of an AUD- and endophenotype-linked *KCNJ6* haplotype on neuronal function, with a goal of identifying mechanisms that could eventually drive therapeutic strategies. To retain the appropriate genetic background for individuals with AUD, we selected subjects from the NIAAA/COGA Sharing Repository, using both *KCNJ6* haplotype and alcohol dependence as criteria (Table 1). By preparing iPSC from these subjects and inducing them to model excitatory neurons, we identified differences in *KCNJ6* mRNA levels and GIRK2 immunoreactivity in individuals with variant *KCNJ6* haplotypes. Gene expression differences predicted effects on neuronal signaling including synaptic function. The *KCNJ6* haplotype was also associated with differences in neuron projection area and membrane excitability, but not in other measures of neuronal differentiation. Surprisingly, we found that ethanol exposure led to increased *KCNJ6* mRNA and GIRK2 expression, paralleled by reduced or eliminated morphological and physiological differences. Reversal of *KCNJ6* haplotype effects by ethanol could also be mimicked by overexpressing GIRK2. These results demonstrate that genetic variants enhancing risk of AUD, even if they do not alter protein sequence, can trigger neuronal mechanisms at the cellular level mirroring or predicting endophenotypes, here ERO, linked with AUD behavior.

Non-coding *KCNJ6* polymorphisms in AUD

Most GWAS SNPs map to non-coding regions of the genome and 3.7% are found in the UTRs[47,48]. The 3′ UTRs of transcripts expressed in brain tend to be longer than those expressed in other tissues and can be involved in post-transcriptional regulation of transcript abundance by affecting RNA stability, translation and/or localization[49,50]. Annotation of *KCNJ6* identifies two transcripts, one with a short 3’ UTR (1,926 bp; ENST00000645093) and one with a substantially longer 3’ UTR (18,112 bp; ENST00000609713). RNAseq coverage analysis in human iN detects only the longer isoform, although it is possible that a relatively small portion could be the shorter isoform, but the uniformly distributed coverage (Fig. 1B) does not indicate this. This longer transcript is orthologous to a 16-kb transcript found in rat brain[51], which includes multiple AU-rich elements, which may affect mRNA stability and could be affected by *KCNJ6* allelic variation. We conclude that the vast majority of *KCNJ6* mRNA is consistent with having the extended 3’ UTR, with the potential for variant SNPs to affect mRNA stability or translation efficiency.

In addition to the three synonymous and intronic SNPs used to select subjects (Table 1), examination of variants in the long 3’UTR by RNAseq alignment predicts linkage of 19 additional SNPs (Fig. 1B; Supplemental Table 1). None of the 3’ UTR SNPs could be mapped uniquely to known regulatory sequences such as predicted microRNA target sites. That is, some SNPs are predicted to destroy or add predicted targeting sites, but all were found in multiple locations within the 3’ UTR, not only where they might be altered by a SNP. It is possible, however, that altered microRNA targeting of one or more sites among many in the 3’UTR could play a role in

426 regulating the stability or translation of the variant *KCNJ6* mRNA, but no clear candidates could
427 be identified for testing.

428 However, results demonstrate that the non-coding haplotype alters expression of GIRK2
429 protein and *KCNJ6* mRNA. iN from subjects with the homozygous variant *KCNJ6* haplotype
430 exhibited lower expression of GIRK2 by immunocytochemistry (Fig. 3D), but while the
431 difference in neuronal mRNA levels as detected by scRNAseq analysis matched this trend, it did
432 not reach significance ($p = 0.0508$; Fig. 1C). FISH analysis, however, confirmed that *KCNJ6* mRNA
433 was reduced in the AF group (Fig. 5J). *KCNJ6* mRNA was also detected in fewer $MAP2^+$ cells and
434 at lower levels per cell (Fig. 5J.b-c). The results of counting GIRK2 puncta and evaluating *KCNJ6*
435 mRNA by scRNAseq and FISH support a diminished expression of GIRK2 in neurons from the
436 affected group. Secondary effects of *KCNJ6* mRNA and GIRK2 protein regulation include many
437 predictors of altered neuronal connectivity and signaling. Genes that were reduced in the AF
438 group (GO:BP Down in Fig. 1E; Supplemental Fig. 3B) point to changes in synaptic transmission
439 and projection morphology. Since we focused on *KCNJ6* haplotype differences in cells without
440 ethanol, we did not expect to match findings in, for example, human AUD brains[52], which found
441 prominent effects in astrocytes and microglia.

442 Surprisingly, ethanol exposure increased expression of both GIRK2 immunoreactivity and *KCNJ6*
443 mRNA. Following 7 days of IEE, GIRK2 puncta in the AF group increased to levels significantly
444 higher than the UN group (Fig. 5B). Similarly, *KCNJ6* mRNA levels were shown to be increased
445 by scRNAseq results (Fig. 1C) and FISH analysis (Fig. 5J). While previous studies identified a
446 binding site for ethanol in a defined pocket of GIRK2[53], suggesting that it could affect protein
447 stabilization, this could not explain the increased mRNA level. There is no indication that
448 ethanol or *KCNJ6* haplotype altered translocation of *KCNJ6* mRNA to neuronal processes (Fig.
449 5J.d-e). Ethanol has been found to affect microRNA expression patterns that regulate
450 mRNA[49,54-59]. It is intriguing to speculate that ethanol might increase expression of GIRK2
451 through this type of mechanism, with polymorphisms in the 3'UTR serving as the modulator.

452 **GIRK2 in the context of alcohol dependence**

453 GIRK channels play an essential role in maintaining the excitability of neurons. For example, in
454 Trisomy 21 individuals, whose cells contain an additional copy of *KCNJ6*, neuronal activity was
455 shown to be reduced due to excessive channel activity[60-62]. On the other hand, loss of GIRK2
456 activity in knockout mice increases susceptibility to induced seizures[20,21]. We detected the
457 presence of GIRK channel function in glutamatergic iNs using the ML297 agonist of GIRK1/2
458 heterotetramers, showing that activation led to a reduction in the frequency of action
459 potentials induced by depolarization (Fig. 2D). However, only 6.7% of neurons responded to
460 ML297, but overexpression of GIRK2 increased the proportion of responding neurons to 30%
461 (Fig. 2D). We therefore chose to focus on evaluating neuronal excitability as an indirect
462 response to changes in GIRK function.

463 By identifying the correlation between GIRK2 expression levels and altered GIRK2-mediated
464 function, we predict that neuronal excitability will be affected by *KCNJ6* variants and alcohol

465 exposure. While GIRK channels play relatively small role in maintaining neuronal homeostasis,
466 modulating GIRK activity to alter cell excitability is predicted to play a critical role. Additionally,
467 downstream effectors of the G protein-mediated signaling pathways presumably regulate
468 neuronal function indirectly[14,15,17,19]. GIRK channels are implicated in several other disorders
469 with abnormal neuronal excitability, including epilepsy, suggesting that they have therapeutic
470 potential[19-21,60-63].

471 **Potential limitations**

472 Factors beyond *KCNJ6* haplotype may contribute to these interpretations. It is possible that the
473 sex of individual neurons might contribute to the results. However, in nearly all parameters
474 tested, there was no difference by sex. scRNAseq identified only 6 genes as different by sex and
475 4 of these are encoded by sex chromosomes. Basal morphology (Fig. 3B, D) was unaffected by
476 sex, but membrane capacitance (Fig. 3F.a, $p = 2.6 \times 10^{-4}$), induced APs (step, Fig. 3G.b, $p =$
477 0.012), and ethanol-treated membrane capacitance (Fig. 5D.a, $p = 3.1 \times 10^{-8}$) all reached
478 significance, although it is difficult to interpret how sex interacts with neuronal function in this
479 context. Finally, we chose to focus on homozygous haplotypes and extreme AUD diagnoses to
480 enhance contrasts, however, additional studies might examine if heterozygotes would exhibit
481 gene dosage effects or be rescued by the presence of the major alleles, similar to
482 endophenotype studies with the original subjects[8].

483 **From genes to behavior**

484 In this study, we found that the variant *KCNJ6* haplotype affects excitability of neurons (Fig. 3 &
485 4E). In Ca^{2+} imaging experiments, concomitant with enhanced excitability in neurons from
486 affected individuals following stimulation with glutamate pulses, we observed an overall
487 increase in basal activity of the neuronal population (Fig. 4F). This is reminiscent of the original
488 observation linking *KCNJ6* variants with an EEG endophenotype, where Kamarajan and
489 colleagues observed that individuals with alcohol dependence and the *KCNJ6* haplotype had an
490 ERO theta power that varied as a function of the *KCNJ6* haplotype in both loss and gain
491 conditions[10]. There is an extensive human literature linking impulsivity to alcohol use
492 problems[64-67]. Impulsivity is elevated in offspring who are at high risk for substance use
493 disorders and may be a reflection of a genetic vulnerability for substance use problems[68].
494 Excitability in individual neurons and particularly in a culture dish of neurons is several levels of
495 complexity removed from EEG patterns in brain. However, our study points to a mechanistic
496 underpinning of how heritable risk traits are likely to play a role in development of unique
497 physiological response to alcohol in the brain.

498

499 # Acknowledgements

500 The Collaborative Study on the Genetics of Alcoholism (COGA), Principal Investigators B.
501 Porjesz, V. Hesselbrock, T. Foroud; Scientific Director, A. Agrawal; Translational Director, D.
502 Dick, includes eleven different centers: University of Connecticut (V. Hesselbrock); Indiana
503 University (H.J. Edenberg, T. Foroud, Y. Liu, M. Plawecki); University of Iowa Carver College of
504 Medicine (S. Kuperman, J. Kramer); SUNY Downstate Health Sciences University (B. Porjesz, J.
505 Meyers, C. Kamarajan, A. Pandey); Washington University in St. Louis (L. Bierut, J. Rice, K.
506 Bucholz, A. Agrawal); University of California at San Diego (M. Schuckit); Rutgers University (J.
507 Tischfield, R. Hart, J. Salvatore); The Children's Hospital of Philadelphia, University of
508 Pennsylvania (L. Almasy); Virginia Commonwealth University (D. Dick); Icahn School of Medicine
509 at Mount Sinai (A. Goate, P. Slesinger); and Howard University (D. Scott). Other COGA
510 collaborators include: L. Bauer (University of Connecticut); J. Nurnberger Jr., L. Wetherill, X.,
511 Xuei, D. Lai, S. O'Connor, (Indiana University); G. Chan (University of Iowa; University of
512 Connecticut); D.B. Chorlian, J. Zhang, P. Barr, S. Kinreich, G. Pandey (SUNY Downstate); N.
513 Mullins (Icahn School of Medicine at Mount Sinai); A. Anokhin, S. Hartz, E. Johnson, V.
514 McCutcheon, S. Saccone (Washington University); J. Moore, Z. Pang, S. Kuo (Rutgers
515 University); A. Merikangas (The Children's Hospital of Philadelphia and University of
516 Pennsylvania); F. Aliev (Virginia Commonwealth University); H. Chin and A. Parsian are the
517 NIAAA Staff Collaborators. We continue to be inspired by our memories of Henri Begleiter and
518 Theodore Reich, founding PI and Co-PI of COGA, and also owe a debt of gratitude to other past
519 organizers of COGA, including Ting- Kai Li, P. Michael Conneally, Raymond Crowe, and Wendy
520 Reich, for their critical contributions. This national collaborative study is supported by NIH
521 Grant U10AA008401 from the National Institute on Alcohol Abuse and Alcoholism (NIAAA) and
522 the National Institute on Drug abuse (NIDA).

Conflict of Interest

The authors declare no conflict of interest.

References

1. Verhulst B, Neale MC, Kendler KS. The heritability of alcohol use disorders: a meta-analysis of twin and adoption studies. *Psychol Med* 2015; **45**(5)**:** 1061-1072.
2. Pollard MS, Tucker JS, Green HD, Jr. Changes in Adult Alcohol Use and Consequences During the COVID-19 Pandemic in the US. *JAMA Network Open* 2020; **3**(9)**:** e2022942-e2022942.
3. Bouza C, Angeles M, Muñoz A, Amate JM. Efficacy and safety of naltrexone and acamprosate in the treatment of alcohol dependence: a systematic review. *Addiction* 2004; **99**(7)**:** 811-828.
4. Heilig M, Egli M. Pharmacological treatment of alcohol dependence: Target symptoms and target mechanisms. *Pharmacology & Therapeutics* 2006; **111**(3)**:** 855-876.
5. Skinner MD, Lahmek P, Pham H, Aubin HJ. Disulfiram efficacy in the treatment of alcohol dependence: a meta-analysis. *PLoS One* 2014; **9**(2)**:** e87366.
6. Salvatore JE, Gottesman, II, Dick DM. Endophenotypes for Alcohol Use Disorder: An Update on the Field. *Curr Addict Rep* 2015; **2**(1)**:** 76-90.
7. Chorlian DB, Rangaswamy M, Manz N, Meyers JL, Kang SJ, Kamarajan C *et al.* Genetic correlates of the development of theta event related oscillations in adolescents and young adults. *Int J Psychophysiol* 2017; **115:** 24-39.
8. Kang SJ, Rangaswamy M, Manz N, Wang JC, Wetherill L, Hinrichs T *et al.* Family-based genome-wide association study of frontal θ oscillations identifies potassium channel gene KCNJ6. *Genes Brain Behav* 2012; **11**(6)**:** 712-719.
9. Clarke TK, Laucht M, Ridinger M, Wodarz N, Rietschel M, Maier W *et al.* KCNJ6 is associated with adult alcohol dependence and involved in gene × early life stress interactions in adolescent alcohol drinking. *Neuropsychopharmacology* 2011; **36**(6)**:** 1142-1148.
10. Kamarajan C, Pandey AK, Chorlian DB, Manz N, Stimus AT, Edenberg HJ *et al.* A KCNJ6 gene polymorphism modulates theta oscillations during reward processing. *Int J Psychophysiol* 2017; **115:** 13-23.
11. Andrew C, Fein G. Event-related oscillations versus event-related potentials in a P300 task as biomarkers for alcoholism. *Alcohol Clin Exp Res* 2010; **34**(4)**:** 669-680.
12. Kamarajan C, Rangaswamy M, Tang Y, Chorlian DB, Pandey AK, Roopesh BN *et al.* Dysfunctional reward processing in male alcoholics: an ERP study during a gambling task. *J Psychiatr Res* 2010; **44**(9)**:** 576-590.
13. Glaaser IW, Slesinger PA. Structural Insights into GIRK Channel Function. *International review of neurobiology* 2015; **123:** 117-160.
14. Luscher C, Slesinger PA. Emerging roles for G protein-gated inwardly rectifying potassium (GIRK) channels in health and disease. *Nat Rev Neurosci* 2010; **11**(5)**:** 301-315.
15. Zhao Y, Gameiro-Ros I, Glaaser IW, Slesinger PA. Advances in Targeting GIRK Channels in Disease. *Trends Pharmacol Sci* 2021; **42**(3)**:** 203-215.
16. Reuveny E, Slesinger PA, Inglese J, Morales JM, Iñiguez-Lluhi JA, Lefkowitz RJ *et al.* Activation of the cloned muscarinic potassium channel by G protein beta gamma subunits. *Nature* 1994; **370**(6485)**:** 143-146.
17. Aryal P, Dvir H, Choe S, Slesinger PA. A discrete alcohol pocket involved in GIRK channel activation. *Nat Neurosci* 2009; **12**(8)**:** 988-995.
18. Bodhinathan K, Slesinger PA. Alcohol modulation of G-protein-gated inwardly rectifying potassium channels: from binding to therapeutics. *Front Physiol* 2014; **5:** 76.

19. Blednov YA, Stoffel M, Chang SR, Harris RA. Potassium channels as targets for ethanol: studies of G-protein-coupled inwardly rectifying potassium channel 2 (GIRK2) null mutant mice. *J Pharmacol Exp Ther* 2001; **298**(2)**:** 521-530.
20. Blednov YA, Stoffel M, Chang SR, Harris RA. GIRK2 deficient mice. Evidence for hyperactivity and reduced anxiety. *Physiol Behav* 2001; **74**(1-2)**:** 109-117.
21. Hill KG, Alva H, Blednov YA, Cunningham CL. Reduced ethanol-induced conditioned taste aversion and conditioned place preference in GIRK2 null mutant mice. *Psychopharmacology (Berl)* 2003; **169**(1)**:** 108-114.
22. Lieberman R, Levine ES, Kranzler HR, Abreu C, Covault J. Pilot study of iPS-derived neural cells to examine biologic effects of alcohol on human neurons in vitro. *Alcohol Clin Exp Res* 2012; **36**(10)**:** 1678-1687.
23. Lieberman R, Kranzler HR, Levine ES, Covault J. Examining the effects of alcohol on GABA(A) receptor mRNA expression and function in neural cultures generated from control and alcohol dependent donor induced pluripotent stem cells. *Alcohol* 2018; **66:** 45-53.
24. Halikere A, Popova D, Scarnati MS, Hamod A, Swerdel MR, Moore JC *et al.* Addiction associated N40D mu-opioid receptor variant modulates synaptic function in human neurons. *Mol Psychiatry* 2020; **25**(7)**:** 1406-1419.
25. Scarnati MS, Boreland AJ, Joel M, Hart RP, Pang ZP. Differential sensitivity of human neurons carrying mu opioid receptor (MOR) N40D variants in response to ethanol. *Alcohol* 2020; **87:** 97-109.
26. Patzke C, Dai J, Brockmann MM, Sun Z, Fenske P, Rosenmund C *et al.* Cannabinoid receptor activation acutely increases synaptic vesicle numbers by activating synapsins in human synapses. *Mol Psychiatry* 2021.
27. Vierbuchen T, Ostermeier A, Pang ZP, Kokubu Y, Sudhof TC, Wernig M. Direct conversion of fibroblasts to functional neurons by defined factors. *Nature* 2010; **463**(7284)**:** 1035-1041.
28. Pang ZP, Yang N, Vierbuchen T, Ostermeier A, Fuentes DR, Yang TQ *et al.* Induction of human neuronal cells by defined transcription factors. *Nature* 2011; **476**(7359)**:** 220-223.
29. Zhang Y, Pak C, Han Y, Ahlenius H, Zhang Z, Chanda S *et al.* Rapid single-step induction of functional neurons from human pluripotent stem cells. *Neuron* 2013; **78**(5)**:** 785-798.
30. Lin HC, He Z, Ebert S, Schörnig M, Santel M, Nikolova MT *et al.* NGN2 induces diverse neuron types from human pluripotency. *Stem Cell Reports* 2021; **16**(9)**:** 2118-2127.
31. Bardy C, van den Hurk M, Eames T, Marchand C, Hernandez RV, Kellogg M *et al.* Neuronal medium that supports basic synaptic functions and activity of human neurons in vitro. *Proc Natl Acad Sci U S A* 2015; **112**(20)**:** E2725-2734.
32. Schneider CA, Rasband WS, Eliceiri KW. NIH Image to ImageJ: 25 years of image analysis. *Nature methods* 2012; **9**(7)**:** 671-675.
33. Fantuzzo JA, Robles DA, Mirabella VR, Hart RP, Pang ZP, Zahn JD. Development of a high-throughput arrayed neural circuitry platform using human induced neurons for drug screening applications. *Lab Chip* 2020; **20**(6)**:** 1140-1152.
34. Bates D, Mächler M, Bolker B, Walker S. Fitting Linear Mixed-Effects Models Using lme4. *Journal of Statistical Software* 2015; **67**(1)**:** 1 - 48.
35. Højsgaard S, Halekoh U, Yan J. The R Package geepack for Generalized Estimating Equations. *Journal of Statistical Software* 2005; **15**(2)**:** 1 - 11.
36. Love MI, Huber W, Anders S. Moderated estimation of fold change and dispersion for RNA-seq data with DESeq2. *Genome Biol* 2014; **15**(12)**:** 550.
37. Mitchell JM, Nemesh J, Ghosh S, Handsaker RE, Mello CJ, Meyer D *et al.* Mapping genetic effects on cellular phenotypes with “cell villages”. *bioRxiv* 2020**:** 2020.2006.2029.174383.

38. Lesage F, Guillemare E, Fink M, Duprat F, Heurteaux C, Fosset M *et al.* Molecular properties of neuronal G-protein-activated inwardly rectifying K+ channels. *J Biol Chem* 1995; **270**(48)**:** 28660-28667.
39. Ang CE, Wernig M. Induced neuronal reprogramming. *J Comp Neurol* 2014; **522**(12)**:** 2877-2886.
40. Shelby H, Shelby T, Wernig M. Somatic Lineage Reprogramming. *Cold Spring Harb Perspect Biol* 2021.
41. Kang HM, Subramaniam M, Targ S, Nguyen M, Maliskova L, McCarthy E *et al.* Multiplexed droplet single-cell RNA-sequencing using natural genetic variation. *Nat Biotechnol* 2018; **36**(1)**:** 89-94.
42. Marron Fernandez de Velasco E, Zhang L, B NV, Tipps M, Farris S, Xia Z *et al.* GIRK2 splice variants and neuronal G protein-gated K(+) channels: implications for channel function and behavior. *Sci Rep* 2017; **7**(1)**:** 1639.
43. Wydeven N, Marron Fernandez de Velasco E, Du Y, Benneyworth MA, Hearing MC, Fischer RA *et al.* Mechanisms underlying the activation of G-protein-gated inwardly rectifying K+ (GIRK) channels by the novel anxiolytic drug, ML297. *Proc Natl Acad Sci U S A* 2014; **111**(29)**:** 10755-10760.
44. Days E, Kaufmann K, Romaine I, Niswender C, Lewis M, Utley T *et al.* Discovery and Characterization of a Selective Activator of the G-Protein Activated Inward-Rectifying Potassium (GIRK) Channel. *Probe Reports from the NIH Molecular Libraries Program*. National Center for Biotechnology Information (US): Bethesda (MD), 2010.
45. Kang S, Chen X, Gong S, Yu P, Yau S, Su Z *et al.* Characteristic analyses of a neural differentiation model from iPSC-derived neuron according to morphology, physiology, and global gene expression pattern. *Scientific reports* 2017; **7**(1)**:** 12233.
46. Chen TW, Wardill TJ, Sun Y, Pulver SR, Renninger SL, Baohan A *et al.* Ultrasensitive fluorescent proteins for imaging neuronal activity. *Nature* 2013; **499**(7458)**:** 295-300.
47. Steri M, Idda ML, Whalen MB, Orrù V. Genetic variants in mRNA untranslated regions. *Wiley Interdiscip Rev RNA* 2018; **9**(4)**:** e1474.
48. Wang D, Liu S, Warrell J, Won H, Shi X, Navarro FCP *et al.* Comprehensive functional genomic resource and integrative model for the human brain. *Science* 2018; **362**(6420).
49. Nunez YO, Mayfield RD. Understanding Alcoholism Through microRNA Signatures in Brains of Human Alcoholics. *Front Genet* 2012; **3:** 43.
50. Wehrspaun C, Ponting C, Marques A. Brain-expressed 3′UTR extensions strengthen miRNA cross-talk between ion channel/transporter encoding mRNAs. *Frontiers in Genetics* 2014; **5**(41).
51. Suda S, Nibuya M, Suda H, Takamatsu K, Miyazaki T, Nomura S *et al.* Potassium channel mRNAs with AU-rich elements and brain-specific expression. *Biochem Biophys Res Commun* 2002; **291**(5)**:** 1265-1271.
52. Brenner E, Tiwari GR, Kapoor M, Liu Y, Brock A, Mayfield RD. Single cell transcriptome profiling of the human alcohol-dependent brain. *Hum Mol Genet* 2020; **29**(7)**:** 1144-1153.
53. Bodhinathan K, Slesinger PA. Molecular mechanism underlying ethanol activation of G-protein-gated inwardly rectifying potassium channels. *Proc Natl Acad Sci U S A* 2013; **110**(45)**:** 18309-18314.
54. Sathyan P, Golden HB, Miranda RC. Competing interactions between micro-RNAs determine neural progenitor survival and proliferation after ethanol exposure: evidence from an ex vivo model of the fetal cerebral cortical neuroepithelium. *J Neurosci* 2007; **27**(32)**:** 8546-8557.
55. Pietrzykowski AZ, Friesen RM, Martin GE, Puig SI, Nowak CL, Wynne PM *et al.* Posttranscriptional regulation of BK channel splice variant stability by miR-9 underlies neuroadaptation to alcohol. *Neuron* 2008; **59**(2)**:** 274-287.

56. Lewohl JM, Nunez YO, Dodd PR, Tiwari GR, Harris RA, Mayfield RD. Up-regulation of microRNAs in brain of human alcoholics. *Alcohol Clin Exp Res* 2011; **35**(11)**:** 1928-1937.
57. Osterndorff-Kahanek EA, Tiwari GR, Lopez MF, Becker HC, Harris RA, Mayfield RD. Long-term ethanol exposure: Temporal pattern of microRNA expression and associated mRNA gene networks in mouse brain. *PLoS One* 2018; **13**(1)**:** e0190841.
58. Lim Y, Beane-Ebel JE, Tanaka Y, Ning B, Husted CR, Henderson DC *et al.* Exploration of alcohol use disorder-associated brain miRNA-mRNA regulatory networks. *Translational psychiatry* 2021; **11**(1)**:** 504.
59. Zhu S, Wu J, Hu J. Non-coding RNA in alcohol use disorder by affecting synaptic plasticity. *Exp Brain Res* 2022.
60. Best TK, Siarey RJ, Galdzicki Z. Ts65Dn, a mouse model of Down syndrome, exhibits increased GABAB-induced potassium current. *J Neurophysiol* 2007; **97**(1)**:** 892-900.
61. Harashima C, Jacobowitz DM, Witta J, Borke RC, Best TK, Siarey RJ *et al.* Abnormal expression of the G-protein-activated inwardly rectifying potassium channel 2 (GIRK2) in hippocampus, frontal cortex, and substantia nigra of Ts65Dn mouse: a model of Down syndrome. *J Comp Neurol* 2006; **494**(5)**:** 815-833.
62. Reeves RH, Irving NG, Moran TH, Wohn A, Kitt C, Sisodia SS *et al.* A mouse model for Down syndrome exhibits learning and behaviour deficits. *Nat Genet* 1995; **11**(2)**:** 177-184.
63. Kleschevnikov AM, Yu J, Kim J, Lysenko LV, Zeng Z, Yu YE *et al.* Evidence that increased Kcnj6 gene dose is necessary for deficits in behavior and dentate gyrus synaptic plasticity in the Ts65Dn mouse model of Down syndrome. *Neurobiol Dis* 2017; **103:** 1-10.
64. Congdon E, Canli T. The endophenotype of impulsivity: reaching consilience through behavioral, genetic, and neuroimaging approaches. *Behav Cogn Neurosci Rev* 2005; **4**(4)**:** 262-281.
65. Dick DM, Smith G, Olausson P, Mitchell SH, Leeman RF, O'Malley SS *et al.* Understanding the construct of impulsivity and its relationship to alcohol use disorders. *Addict Biol* 2010; **15**(2)**:** 217-226.
66. Sher KJ, Trull TJ. Personality and disinhibitory psychopathology: alcoholism and antisocial personality disorder. *J Abnorm Psychol* 1994; **103**(1)**:** 92-102.
67. Verdejo-García A, Lawrence AJ, Clark L. Impulsivity as a vulnerability marker for substance-use disorders: review of findings from high-risk research, problem gamblers and genetic association studies. *Neurosci Biobehav Rev* 2008; **32**(4)**:** 777-810.
68. Polich J, Bloom FE. P300, alcoholism heritability, and stimulus modality. *Alcohol* 1999; **17**(2)**:** 149-156.
69. Cáceres A, Banker GA, Binder L. Immunocytochemical localization of tubulin and microtubule-associated protein 2 during the development of hippocampal neurons in culture. *J Neurosci* 1986; **6**(3)**:** 714-722.
70. Ma F, Xu J, Liu Y, Popova D, Youssef MM, Hart RP *et al.* The amyloid precursor protein modulates the position and length of the axon initial segment offering a new perspective on Alzheimer's disease genetics. *bioRxiv* 2022**:** 2022.2001.2023.477413.

718 # Figure Legends

719 **Figure 1. Experimental design and gene expression analysis**
720 **A.** Diagram outlining experimental design. Lymphocytes from subjects with or without AUD
721 diagnosis and *KCNJ6* haplotype variants were selected, reprogrammed into iPSC, induced into
722 excitatory iNs, and analyzed by morphometry, immunocytochemistry, gene expression, and
723 electrophysiology. **B.** Sequencing alignment and depth analysis of bulk RNA sequencing
724 confirmed expression of *KCNJ6* mRNA in iN cultures, specifically the ENST00000609713 isoform,
725 containing an 18.1 kilobase 3'UTR region. *KCNJ6* exons are mapped to chromosome locations
726 (marked in mb, megabases) and the position of the gene is indicated by the red box on the
727 chromosome 21 pictogram, top, with transcription direction on the minus strand indicated by
728 the broken arrow. Variant analysis of RNA sequences predicts a region of linkage disequilibrium
729 of 22 SNPs, including the 3 SNPs used to select subjects (red, Table 1), and 19 additional SNPs
730 (blue, Supplemental Table 1). Depth: number of sequencing reads per base aligned by position.
731 Frequency: thickness of curved lines represents the relative frequency of splice site utilization
732 between exons. **C.** Single-cell RNAseq identifies a cluster of induced neurons (lower left),
733 expressing markers consistent with neuronal function including *SYP*, *SLC17A6*, *GRIN2B*, *SCN3A*,
734 *KCNJ3*, and *KCNJ6*; distinct from "transition neurons" that either do not express these markers
735 or express sporadically. Additional markers are plotted in Supplemental Fig. 2E. Isolating *KCNJ6*
736 mRNA expression, aggregated by subject and treatment, AF neurons expressed a trend towards
737 lower levels than UN neurons ($p = 0.0508$; Wald test), but treatment of 7d with IEE at 20 mM
738 peak concentration increased AF expression above untreated ($p = 0.0225$) to levels similar to
739 UN control ($p = 0.322$, not denoted on figure). **D.** Volcano plot for untreated UN vs AF neurons,
740 highlighting genes significantly different (FDR > 0.05) and at least 1.5-fold changed (red dots).
741 Genes below the fold-change cut-off are marked in green, and those not significantly different
742 are marked in blue. Significantly different genes are listed in Supplemental Table 3. **F.** Gene
743 ontology (GO) enrichment of top 10 biological process (BP) terms for up- or down-regulated
744 genes. Plots indicate the number of regulated genes from the term and the color indicates the
745 adjusted p-value (q-value; key). All enriched terms are listed in Supplemental Tables 4-5.

746 **Figure 2. Validation of GIRK2 expression and function in human induced neurons.**
747 **A**. Representative confocal images of GIRK2 immunoreactivity in mouse cortical neurons.
748 Arrowheads indicate locations of GIRK2-staining puncta, with an example punctum enlarged in
749 the inset, overlapping or adjacent to βIII-tubulin-positive processes. We observed two cellular
750 expression patterns – one where the entire neuron is decorated with GIRK2 antibody
751 (Supplemental Fig. 4), or another where GIRK2 expression is relatively faint and observed
752 mostly on neuronal processes, shown here. **B**. GIRK2 expression patterns in human induced
753 neurons (iNs), showing representative confocal images from line 420. Inset shows two adjacent
754 puncta. GIRK2 immunoreactivity matched a pattern of process-selective expression in mouse
755 (Panel A and Supplemental Fig. 4A), where GIRK2 was detected as relatively small (~ 0.5 µm
756 diameter) puncta scattered primarily along the processes. Localization of GIRK2

757 immunoreactivity in human iN did not directly colocalize with synaptic vesicle marker VGLUT2
758 or synaptic marker Syn1 (Supplemental Fig. 5), but instead was found most frequently adjacent
759 to synapses but overlapping the shafts of the βIII tubulin-positive processes, and less so on
760 MAP2 positive processes (Figs. 2D.a, 3C, 3E). Cultured neurons express βIII tubulin throughout
761 the cell, but not as strongly in axonal processes[69]. We previously found that processes in human
762 iN cells stained for ankyrin G, identifying the axonal initial segment, which similarly lacked βIII-
763 tubulin[70]. Detection of GIRK2 primarily on βIII-tubulin$^+$/MAP$^-$ processes, therefore, suggests pre-
764 axonal, and likely presynaptic, localization. **C**. Following infection of iN cultures with lentivirus
765 expressing both *KCNJ6* and mCherry, large numbers of GIRK2$^+$ puncta are seen in representative
766 images (line 420). **D**. Evaluation of GIRK2 function in iNs, (a) quantification of GIRK2 expression
767 on MAP2$^+$ vs. βIII-tubulin$^+$ neuronal processes. GIRK2 is more abundant on βIII-tubulin
768 processes (p=0.0006, one-tailed Student's t-test, n=15 cells per group, cell line 420). (b) Basal
769 levels (upper pie plot) of the GIRK current in iNs as percent of neurons responding with
770 hyperpolarization to the selective GIRK activator (160 nM ML297); compared with responding
771 percentage when GIRK2 is overexpressed (lower pie chart). (c) Representative image of iN
772 overexpressing GIRK2, as confirmed with mCherry fluorescence. (d) Representative traces of
773 induced action potential firing before and after GIRK activation, demonstrating the contribution
774 of GIRK function to cell excitability. (e) Representative trace of spontaneous postsynaptic
775 potential (sEPSCs) recordings during ML297 (160 nM) GIRK activator wash-in, demonstrating a
776 shift of 7mV holding current (amplifier-dependent compensation of GIRK-mediated membrane
777 hyperpolarization). (f) Quantification of neuronal excitability at baseline and following GIRK
778 activation with 160 nM ML297 (p=0.015, paired Student's t-test, n=9 cells before/after ML297,
779 cell line 376).

780 **Figure 3. Impact of AUD-associated *KCNJ6* haplotype on neuronal properties.**
781 **A**. Principles of morphological analysis of induced neurons: (a) Neurite area was the total TuJ1$^+$
782 (βIII-tubulin)$^+$ staining area outside the cell soma. (b) Solidity is the area of the soma divided by
783 its convex hull area. (c) Soma size was the area of the MAP2$^+$ cell body. (d) Circularity compared
784 the perimeter to the area. **B**. Morphometry of iNs from *KCNJ6* haplotype variant and affected
785 (**AF**, cyan) or unaffected (**UN**, grey) individuals. Results are summed by group (left) or plotted
786 individually by cell line (right), with subjects identified by line number (see Table 1—females
787 identified with grey numbers). Individual cells are plotted as dots with the bar showing the
788 mean, with error bars indicating the standard error of the mean (SEM). No significant
789 differences were found in (a) soma size, (b) circularity, or (c) soma solidity, but total neurite
790 area was increased in the AF group (p =0.018). **C**. Representative images of iNs from individual
791 lines, with arrows identifying individual GIRK2 puncta (red) localized on βIII-tubulin$^+$ processes
792 (gray). **D**. GIRK2 expression was decreased in the AF as measured by puncta counts (a, p =
793 0.0012), circularity (c, p = 0.007), or solidity (d, p = 0.037), while there was no difference in
794 puncta size (b). **E**. Representative images of individual GIRK2 puncta (red) localized on βIII-
795 tubulin$^+$ processes (gray). **F**. Electrophysiological analysis of passive neuronal properties,
796 showing no difference in (a) membrane capacitance (b) membrane resistance, or (c)

797 spontaneous EPSCs frequency. (d) Representative sEPSCs traces for each line. (e) Spontaneous
798 EPSCs amplitude. **G**. Electrophysiological analysis of active neuronal properties. (a)
799 Quantification of current required to shift resting membrane potential to -65mV in pA:
800 difference by group $p = 1.2 \times 10^{-5}$; (b) quantification of maximum number of action potentials
801 (APs) induced with the "step" protocol, p = 0.086; (c) representative traces of APs induced with
802 the "step" protocol; (d) quantification of number of action potentials (APs) induced with the
803 "ramp" protocol, $p = 2.0 \times 10^{-9}$; (e) representative traces of APs induced with the "ramp"
804 protocol. A generalized linear model was used to evaluate group differences for morphometry
805 and GIRK2 expression, and generalized estimation equations was used for electrophysiology
806 results. Numbers of cell lines and replicates for each experiment are shown in Supplemental
807 Table 6.

808 **Figure 4. Evaluation of neuronal excitability in human induced neuron populations.**
809 **A.** Representative epifluorescence images of GcaMP6f expression in iNs from affected (233,
810 246) and unaffected individuals (420, 472). **B, C.** Raster plots of the calcium spiking pattern of
811 representative experiments from unaffected neurons (**B**, individual 472) and affected neurons
812 (**C**, individual 233), under the stimulation protocol used. Green and purple bars show the
813 application of 30 s pulses of Glu 10-50 µM and KCl 18 mM, respectively, on the neuron
814 populations during the stimulation protocol. Arrows show the epochs of the calcium imaging
815 recordings selected for calcium spike quantification: baseline, glutamate pulse 1, and KCl pulse
816 1. **D.** Stimulation protocol (upper bar) and representative raw fluorescence trace (AF individual
817 233) from a complete recording. The zoom-ins on the first glutamate and KCl pulses depict
818 glutamate and KCl elicited activity, respectively. The vertical dotted lines correspond to the
819 calcium spikes detected after analysis. **E, F, G.** Number of spikes per ROI per minute during
820 baseline (**E**, spontaneous activity), glutamate pulse 1 (**F**, glutamate-elicited activity) and KCl
821 pulse 1 (**G**, KCl-elicited activity). The pie charts represent the proportion of neurons of UN (grey)
822 and AF (blue) individuals that exhibited a certain number of calcium spikes during each three
823 epochs of the recording. The bar plots show the number of spikes per ROI per minute fired by
824 unaffected individuals (grey) and affected individuals (blue) during baseline, glutamate pulse 1
825 and KCl pulse 1. The sample size is depicted in the bar of each group as number of iN
826 batches/number of experiments/number of neurons. Differences between affected and unaffected
827 groups were evaluated by two-tailed unpaired Student's t-test (Welch's correction for non-equal SD, **p
828 < 0.01, ****p < 0.0001).

829 **Figure 5. Ethanol treatment reduced *KCNJ6* haplotype differences in iN excitability and GIRK2**
830 **expression.**
831 **A**. Morphological analysis of IEE iNs generated from affected and unaffected individuals,
832 showing no difference in: (a) neuronal soma size (p = 0.32); (b) soma circularity (p = 0.54); (c)
833 soma solidity (p = 0.92); and (d) total neurite area (p = 0.98). **B**. There was no difference in
834 GIRK2 expression in the IEE AF group iNs compared with UN by (a) puncta counts (p = 0.46), (b)
835 puncta size (p = 0.36), (c) puncta circularity (p = 0.052), or (d) solidity (p = 0.47). **C.**
836 Representative images of individual GIRK2 puncta (red) localized on βIII-Tubulin positive

837 processes (gray) for each cell line. **D**. Electrophysiological analysis of passive neuronal
838 properties in IEE iNs, showing (a) a small decrease in AF membrane capacitance ($p = 9.6 \times 10^{-9}$),
839 but no difference in (b) membrane resistance ($p = 0.63$), (c) spontaneous EPSCs frequency ($p =$
840 0.32), or (d) spontaneous EPSCs amplitude ($p = 0.19$). (e) Representative sEPSCs traces for each
841 cell line. (f) The AF group exhibited no change in resting membrane potential after IEE ($p =$
842 0.79). **E**. Electrophysiological analysis of active neuronal properties found no difference in IEE
843 iNs for (a) current required to shift resting membrane potential to -65mV ($p = 0.32$), (b)
844 maximum number of action potentials (APs) induced with the "step" protocol ($p = 0.48$), with
845 (c) representative traces of APs induced with the "step" protocol, (d) number of action
846 potentials (APs) induced with the "ramp" protocol ($p = 0.95$), with (e) representative traces of
847 APs induced with the "ramp" protocol. **F**. Representative images from individual lines of iNs,
848 exposed to 7d of IEE, marked with arrows pointing to individual GIRK2 puncta (red) localized on
849 βIII-Tubulin positive processes (gray). **G**. Summarized results from all lines showing differences
850 in GIRK2 expression levels before and after 7 days of 20 mM IEE with ethanol (EtOH; $p = 1.0 \times$
851 10^{-20}). **H.** Representative images of individual GIRK2 puncta (red) localized on βIII-Tubulin
852 positive processes (gray) prior and following 7 days 20 mM IEE with ethanol. Sample images are
853 from line 246. **I.** Representative images of FISH detection of *KCNJ6* mRNA for each cell line. **J.**
854 Quantification of FISH. (a) The number of *KCNJ6* puncta normalized to the number of cells in an
855 image shows decreased expression in control AF compared with UN ($p = 8.2 \times 10^{-3}$), increased
856 expression following IEE ($p = 8.2 \times 10^{-3}$; using Tukey's pairwise comparisons). (b) The percentage
857 of *KCNJ6*-expressing $MAP2^{+}$ cells substantially increase in the (c) AF group but not in the (b) UN
858 group. Numbers of *KCNJ6* puncta were analyzed by expression levels per cell, as recommended
859 by the FISH manufacturer in (d) UN or (e) AF cells. (f) *KCNJ6* puncta within the neuronal soma
860 show increases following IEE in both UN and AF groups ($p = 0.006$ for genotype, Tukey's post-
861 hoc for UN, $p = 0.01$, for AF, $p = 0.01$). (g) A similar analysis of non-somatic puncta, presumably
862 within neurites, showed no differences following IEE between genotypes ($p=0.23$).

863 **Figure 6. GIRK2 overexpression mimics ethanol response**
864 **A.** Current required to shift resting membrane potential to -65mV, in untreated (control, $p = 5.9$
865 $\times 10^{-4}$), lentiviral *KCNJ6* overexpression (over., $p = 0.23$), or 1 d 20 mM IEE (EtOH, $p = 0.75$)
866 cultures. **B.** Representative traces of APs induced with the "ramp" protocol. **C.** Quantification of
867 maximum number of action potentials (APs) induced with "ramp" protocol, control ($p = 6.8 \times$
868 10^{-6}), overexpression ($p = 0.014$), or 1 d 20 mM IEE ($p = 0.10$). **D.** quantification of GIRK2 puncta
869 after overexpression (line 376, one-tailed Student's t-test $p = 0.04$).

870

871 # Supplementary Materials

872 **Supplemental Tables 1-6:** https://doi.org/10.6084/m9.figshare.19798882.v2

873 **Supplemental Table 1. SNPs identified in RNAseq samples.** Variants were identified in the
874 region surrounding KCNJ6 (chr21: 37499112-38245792) using samtools mpileup to bcftools call,
875 followed by filtering to remove low quality. Results were loaded into the Ensembl VEP tool. A
876 dot (".") indicates missing data and/or low quality. The reference allele and alternate alleles
877 were obtained from the UCSC Genome Table Browser.

878 **Supplemental Table 2: CellRanger parameters for scRNAseq libraries.** Output from CellRanger
879 shows the alignment statistics and numbers of reads confidently mapped.

880 **Supplemental Table 3. Differentially expressed genes (DEG) comparing AF to UN without**
881 **exposure to ethanol.** The table contains all output from DESeq2 results. Excel filters are set to
882 show only genes significantly different (padj <= 0.05) and at least 1.5-fold different
883 (abs(log2FoldChange) > 0.585). Release the filters to see the full list.

884 **Supplemental Table 4. Enriched Gene Ontology-Biological Process (GO-BP) terms from genes**
885 **increased in AF relative to UN.**

886 **Supplemental Table 5. Enriched Gene Ontology-Biological Process (GO-BP) terms from genes**
887 **decreased in AF relative to UN.**

888 **Supplemental Table 6. Numbers of replicates.** For each parameter tested with statistics, the
889 numbers of cells and/or microscope fields is indicated and labeled by Figure numbers/letters.

890 **Supplemental Methods and Figures:** https://doi.org/10.6084/m9.figshare.19798873.v5

891

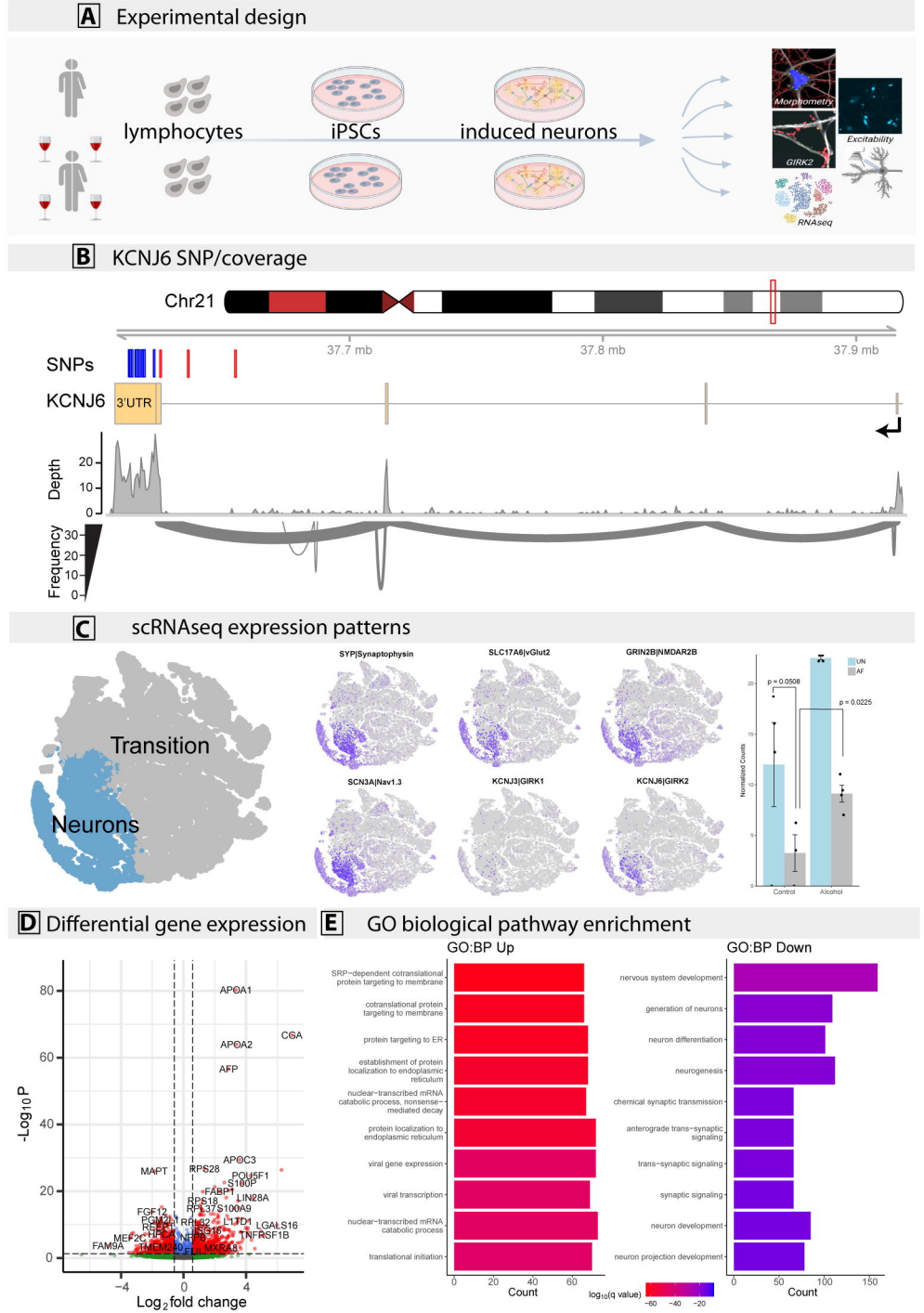

Figure 1, Popova et al., 2022

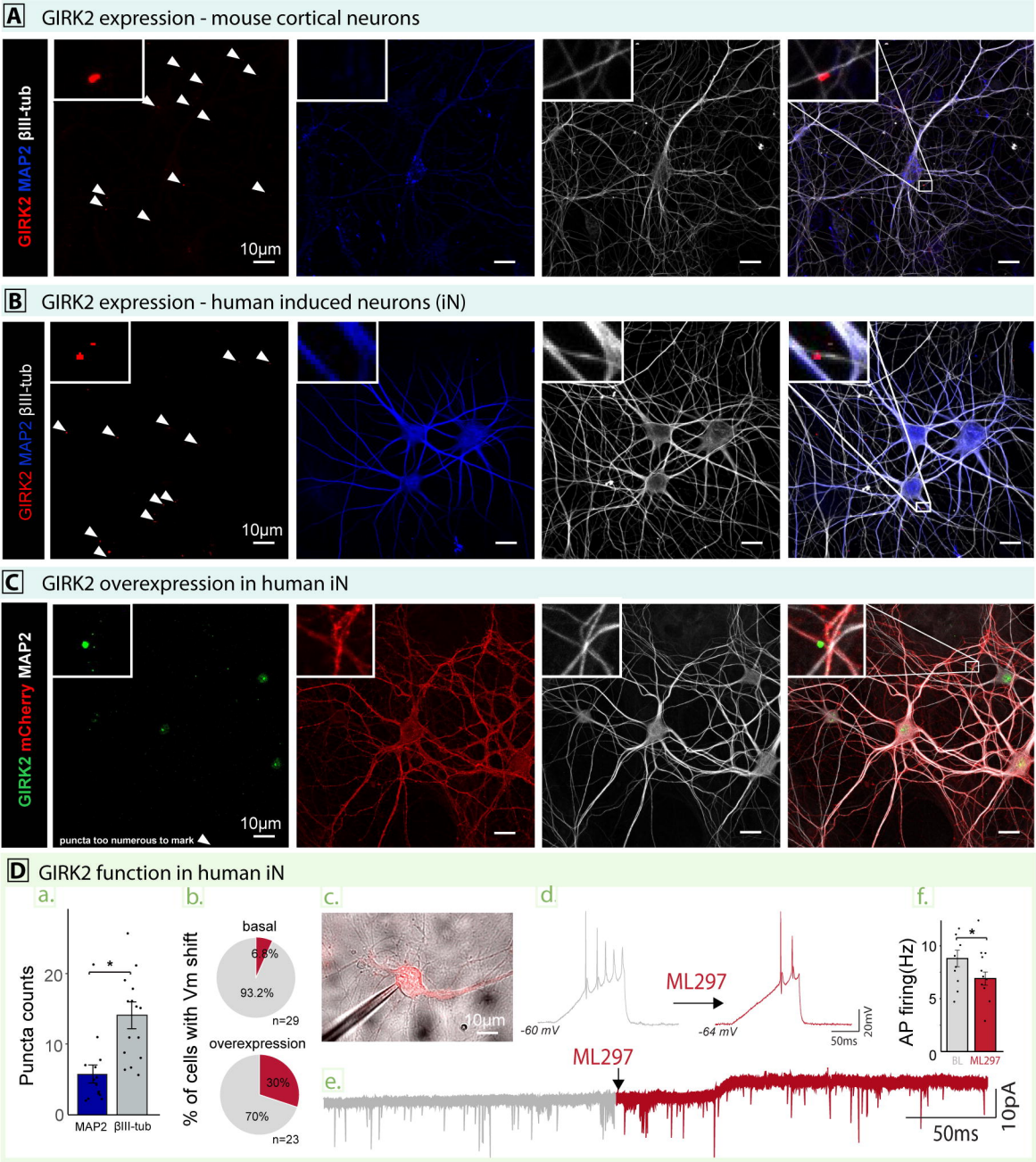

Figure 2, Popova et al., 2022

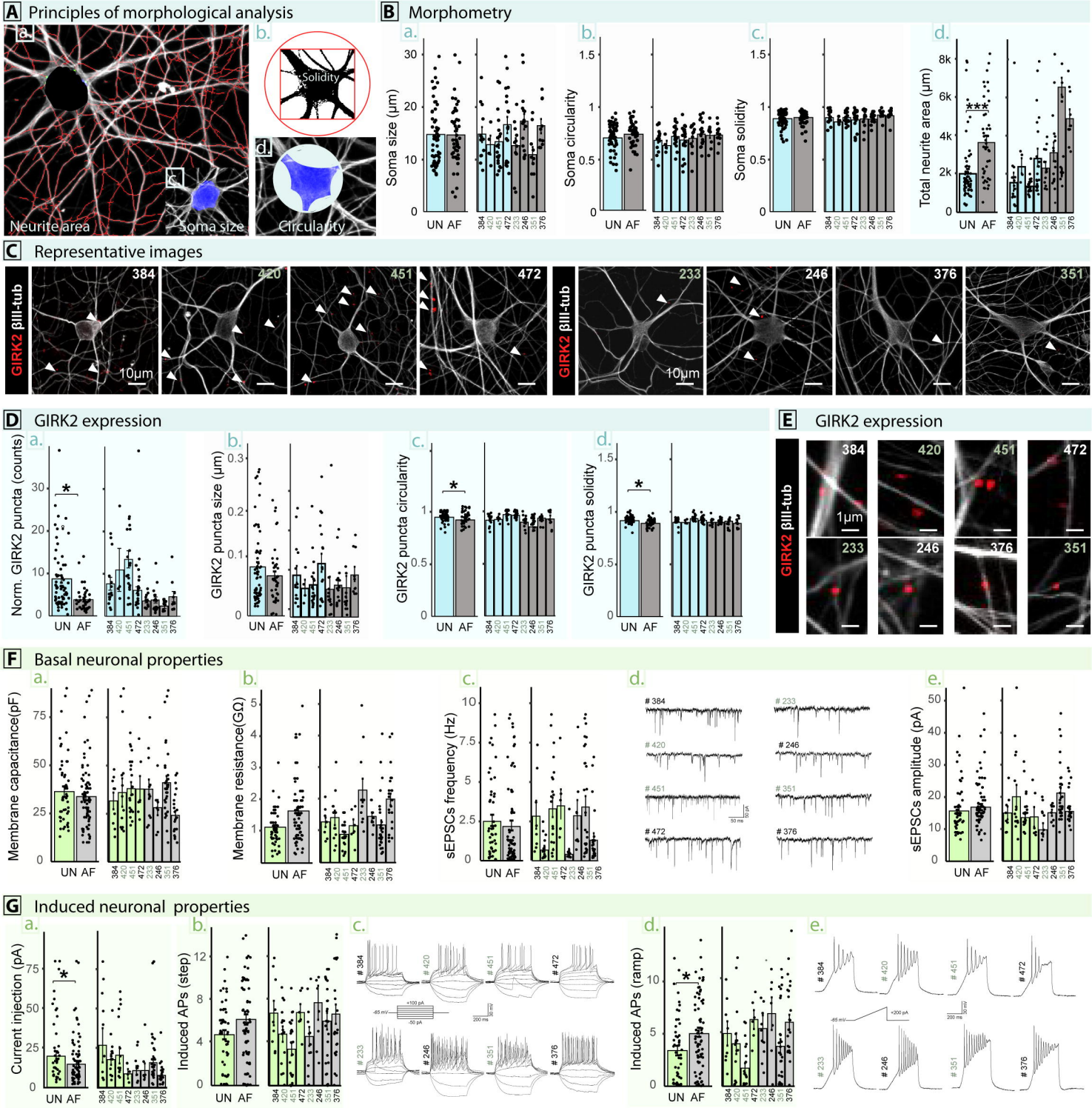

Figure 3, Popova et al., 2022

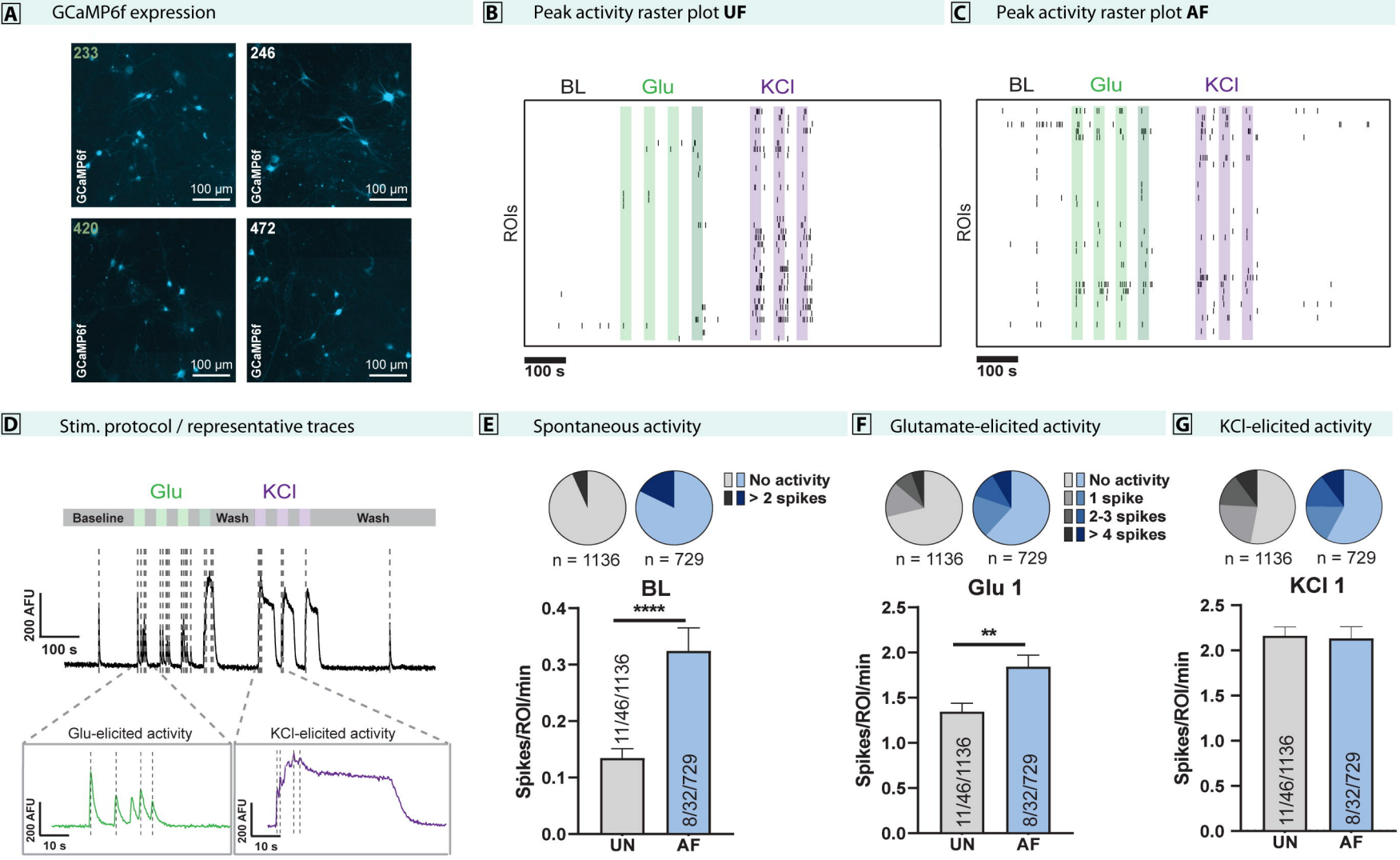

Figure 4, Popova et al., 2022

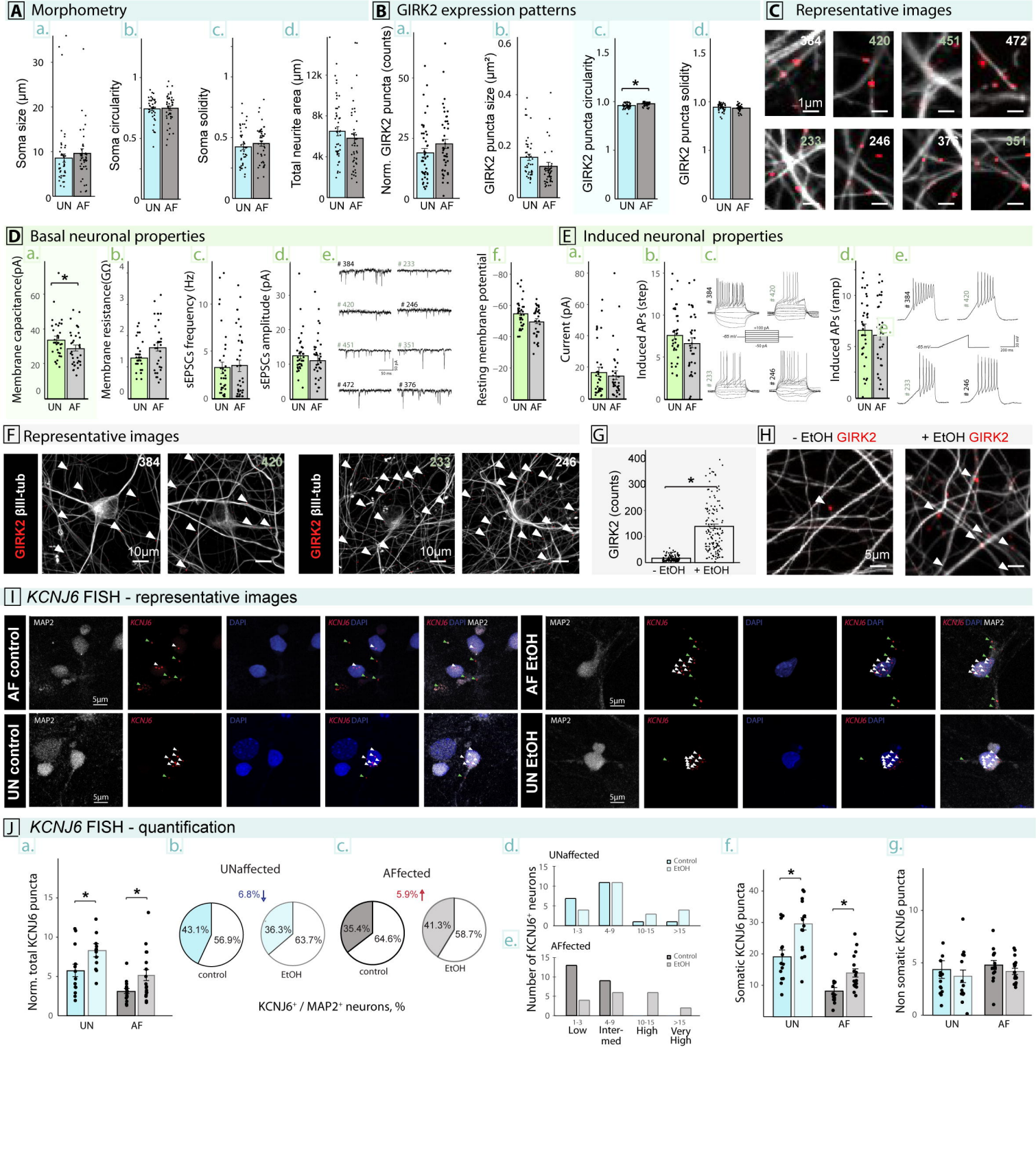

Figure 5, Popova et al., 2022

Active neuronal properties

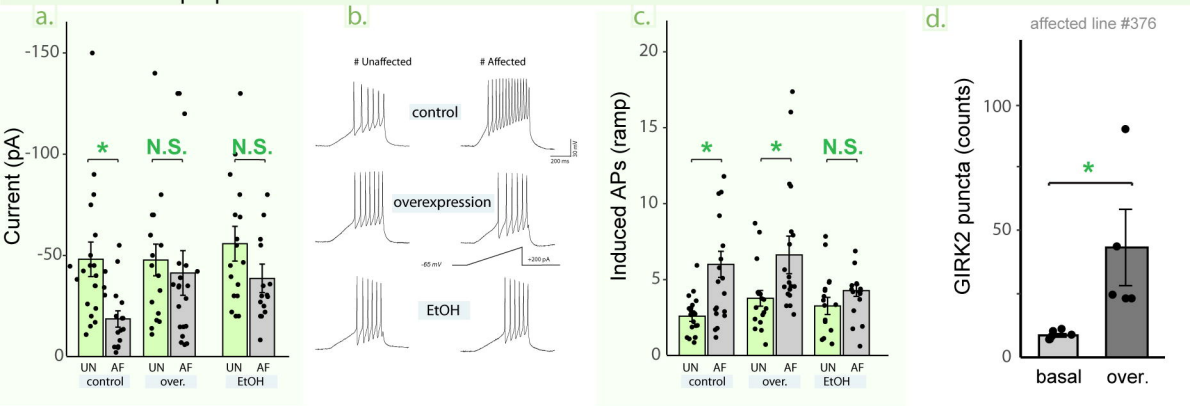

Figure 6, Popova et al., 2022